Pushing forward jet substructure measurements in heavy-ion collisions

Daniel Pablos[1,*] and Alba Soto-Ontoso[2,3,†]

[1]*INFN, Sezione di Torino, via Pietro Giuria 1, I-10125 Torino, Italy*
[2]*Université Paris-Saclay, CNRS, CEA, Institut de physique théorique, 91191 Gif-sur-Yvette, France*
[3]*Theoretical Physics Department, CERN, 1211 Geneva 23, Switzerland*

(Received 28 November 2022; accepted 12 April 2023; published 3 May 2023)

Energetic jets that traverse the quark-gluon plasma created in heavy-ion collisions serve as excellent probes to study this new state of deconfined QCD matter. Presently, however, our ability to achieve a crisp theoretical interpretation of the crescent number of jet observables measured in experiments is hampered by the presence of selection biases. The aim of this work is to minimize those selection biases associated to the modification of the quark- versus gluon-initiated jet fraction in order to assess the presence of other medium-induced effects, namely, color decoherence, by exploring the rapidity dependence of jet substructure observables. So far, all jet substructure measurements at midrapidity have shown that heavy-ion jets are narrower than vacuum jets. We show both analytically and with Monte Carlo simulations that if the narrowing effect persists at forward rapidities, where the quark-initiated jet fraction is greatly increased, this could serve as an unambiguous experimental observation of color decoherence dynamics in heavy-ion collisions.

DOI: 10.1103/PhysRevD.107.094003

I. INTRODUCTION

Ultrarelativistic heavy-ion collisions have succeeded in recreating the extreme temperature and pressure conditions that our Universe experienced during the first microseconds after the big bang. Unraveling the microscopic properties of the medium that permeated our Universe during this epoch, namely, the quark-gluon plasma (QGP), is one of the long-standing questions of particle physics [1,2]. A widely used approach to this challenge is to study the modification of high-momentum particles, or jets, when traversing the QGP, very much like in the Rutherford experiment. Data recorded during the past two decades at both RHIC [3–5] and the LHC [6–9] have confirmed that the interaction between jets and the QGP leads to an overall depletion of the jet yield at high p_t. Theoretically, this suppression, commonly known as *jet quenching* [10–12], is understood as a result of the wide-angle nature of medium-induced emissions which end up being radiated outside of the jet cone and, thus, lead to a net energy loss.

Aiming at a more detailed picture of the multiscale evolution of jets in the presence of a thermal medium, experimental measurements in the past five years have explored jet substructure observables such as the momentum sharing fraction or the opening angle of a pair of *hard* subjets [13–15]. We refer the reader to Ref. [16] for a comprehensive review of the latest jet measurements. These observables can be designed such that the perturbative part of the radiation phase space dominates and are, consequently, under better theoretical control than global ones. Recently, the potential of jet substructure observables beyond the jet declustering tree, namely, energy-energy correlators [17], to unveil color coherence dynamics in heavy-ion collisions has been assessed [18]. Up to now, a varied set of jet substructure measurements has revealed an overall narrowing of the jet core with respect to the vacuum baseline [15,19]. However, the current experimental precision is not high enough to discriminate between disparate theoretical models. In this paper, we develop a strategy that shall allow future measurements to identify the actual physical mechanism behind the observed narrowing effect.

The first model, introduced in Ref. [20], argues that the experimental trend is driven by a larger number of quark-initiated jets, known to be more collimated, after the p_t selection cut in the Pb + Pb sample with respect to $p + p$. An enhanced quark fraction in Pb + Pb could originate from a combination of the color charge dependence of jet quenching and the jet spectrum. That is, since gluon jets

*daniel.pablos.alfonso@to.infn.it
†alba.soto.ontoso@cern.ch

radiate more, they will lose more energy and, as a consequence of the steeply falling spectrum, will not pass the jet p_t selection cut. A critical feature of this model is that if one fixes the color charge of the jet initiator, no modifications are expected with respect to vacuum jet evolution (modulo any potential p_t dependence of the observable itself). The natural question is how different the q/g fractions need to be in order to quantitatively describe the data or, equivalently, how much stronger is the quenching that gluon jets experience. The authors of Ref. [21] achieved a quantitative description of jet substructure observables (see Refs. [15,22]) with a factor of 4 more quark jets in Pb + Pb with respect to $p + p$. Since this number was extracted via a global fit to jet spectrum data [23] (see Figs. 3 and 4 in Ref. [23]), it is agnostic to the dynamics of energy loss.[1] Thus, the physical mechanism that would lead to such a dramatic quenching of gluon jets, far larger than that expected from Casimir scaling,[2] remains to be settled. Throughout the rest of this paper, we will refer to this hypothesis as the "modified q/g fraction model," and we will elaborate more on it in Secs. III A 1 and III C.

An alternative explanation to the narrowing effect relies on the existence of a critical resolution angle of the QGP. This angular scale, defined as $\theta_c = 2/\sqrt{\hat{q}L^3}$ with $\hat{q}$ being the quenching parameter and L the medium length, naturally emerges when considering the soft radiation pattern of an antenna in the multiple soft scattering approximation [28–33] and splits the radiation phase space into resolved and unresolved emissions.[3] In short, if the opening angle of a vacuumlike splitting is larger than θ_c, its two prongs behave as independent emitters of medium-induced gluons. On the contrary, collinear branchings with $\theta < \theta_c$ are not resolved by the medium and, thus, lose energy coherently as an individual color charge. Therefore, jets with $\theta > \theta_c$ are more quenched, leading to an overall narrowing of the jet sample. Two jet-quenching Monte Carlo simulations that incorporate some notion of color coherence, namely, JetMed [39,40] and the hybrid strong-weak coupling model [41–43], are able to quantitatively describe jet substructure data.[4] Naturally, these two models are also sensitive to the different degrees of quenching of quark and gluon jets. However, a purely coherent description of energy loss in these models is not sufficient to match the experimental data, and, thus, a resolution criterion in terms of a critical angle or length is required.

This paper addresses the question on how to experimentally disentangle between the modified q/g fraction and "color decoherence" models. Our strategy is to explore the rapidity dependence of jet substructure observables. For simplicity, we focus on the k_t distribution of the hardest splitting in a jet, but our conclusions apply to any jet substructure measurement.[5] The idea is based on a simple observation: Increasing the jet rapidity enhances the fraction of quark-initiated jets. For a fixed color charge of the jet initiator, the two models under study lead to dramatically different predictions for the k_t distribution. On the one hand, as we have already anticipated, the modified q/g fraction heavy-ion result would approach the vacuum one when moving to forward rapidities, since the ensemble is dominated by quark-initiated jets in both collision systems. In contrast, if the medium is able to resolve the substructure fluctuations developed during the Dokshitzer-Gribov-Lipatov-Altarelli-Parisi (DGLAP) evolution of the jet, the k_t distribution would differ from the $p + p$ baseline for every rapidity bin, as both quark- and gluon-initiated jets feature wide ($\theta > \theta_c$) and narrow ($\theta < \theta_c$) configurations.

In this work, we study the rapidity dependence of the leading-k_t distribution up to $|y| = 4.5$. Experimentally, jet substructure measurements at such forward rapidities are rather challenging and require dedicated instrumentation. For this reason, we deem necessary to address the feasibility of the proposed measurements, both with the current data and in the upcoming high-luminosity phase of the LHC (HL-LHC).[6] The ATLAS Collaboration has pioneered the study of the rapidity dependence of jet quenching by measuring both the inclusive jet spectrum [8] and the fragmentation function [49] at $|y| < 2.8$ and $|y| < 2.1$, respectively. CMS has explored even more forward kinematics and measured the jet cross section in the pseudorapidity region $-6.6 < \eta < -5.2$ using CASTOR [50,51], but only in p + Pb collisions. Similarly, the LHCb detector allows for the reconstruction of charged and neutral particles in the very forward rapidity region ($2 < |y| < 4.5$), but, to this date, heavy-ion measurements were limited to peripheral collisions, where medium effects are expected to be reduced. It is then possible to measure the leading-k_t distribution in both $p + p$ and Pb + Pb collisions with the current

[1]This quark fraction is in tension with the one extracted in Ref. [24] that corresponds to 1.5 increase [see Figs. 1(c) and 1(f)], although an apples-to-apples comparison is not possible due to the different jet selections used in those studies. Experimentally, no sizable modification of the quark and gluon fractions has been observed [25,26].

[2]Casimir scaling is violated, even in vacuum, beyond leading order as was shown in Ref. [27].

[3]A resolution scale also appears when calculating the gluon emission pattern of an antenna using the opacity expansion formalism [34–36], particularly relevant for thin media [37,38].

[4]The JEWEL Monte Carlo [45,46] model also gives a similarly accurate description of this dataset. In terms of color coherence, JEWEL implements a fully resolved picture of energy loss, and, thus, it is expected to give similar results as the hybrid model setting the resolution length L_{res} to zero.

[5]Since $k_t = z\theta$ and the z distribution is barely modified in heavy-ion collisions, the observed narrowing in terms of θ is directly translated into a shift toward smaller k_t. Preliminary experimental results on k_t can be found in Ref. [47].

[6]Although not addressed in this work, we note that the STAR detector will undergo a forward rapidity upgrade [48].

technology of both ATLAS and CMS using charged, high-p_t jets up to $|y| = 2.5$ with data recorded during runs 2 and 3.

As we show below, this rapidity interval could be enough, for jets at sufficiently high p_t, to disentangle between the theoretical models studied in this paper. However, more stringent constraints on the two confronting pictures can be obtained by pushing the measurements to even larger rapidities. This can be achieved in the future HL-LHC, where an integrated luminosity of about $\mathcal{L} = 10$ nb^{-1} in Pb + Pb collisions at a center-of-mass of energy of 5.5 TeV per nucleon pair will be delivered [52]. A further increase in the integrated luminosity is expected in case the heavy-ion program is extended up to the end of run 6, as recently proposed by the ALICE3 experiment [53]. In fact, this detector would be ideal for this study, since it is designed to cover eight units in rapidity with very good tracking and p_t resolution of charged particles [53]. Upgrades in both ATLAS and CMS will also extend their rapidity coverage [54,55], and LHCb plans to extend its centrality coverage to semicentral collisions in run 3 and central collisions in run 4 [52]. To sum up, we consider two experimental settings: (i) "current LHC," which includes measurements up to $|y| < 2.5$, and (ii) "future LHC," where we study jet rapidities as high as $|y| = 4.5$.

The rest of the paper is organized as follows. In Sec. II, we consider dijet events in $p + p$ collisions and study the rapidity dependence of (i) quark and gluon fractions, (ii) the jet p_t spectrum, and (iii) the leading-k_t distribution using PYTHIA [56]. We also provide an analytic estimate of the vacuum k_t distribution. Next, in Sec. III, we explore the modification of all these observables when including medium effects, both analytically (Sec. III A) and with Monte Carlo simulations (Secs. III B and III C). We calculate the medium-modified k_t distribution within two different semianalytic approaches. One model is based on the modified q/g fraction picture, and the results are displayed in Sec. III A 1. The second model, presented in Sec. III A 2, incorporates the dynamics of color decoherence, in a similar fashion as Ref. [57]. For the numerical results, we pursue two paths. In Sec. III B, we use the hybrid Monte Carlo model to study the rapidity dependence of jet suppression and to predict the rapidity dependence of the leading-k_t distribution. Next, in Sec. III C, we present an implementation of the modified q/g fraction model in which PYTHIA is used to obtain the vacuum distributions that are then combined within the logic of a fully coherent energy loss model. We conclude with a summary of the main results of this manuscript in Sec. IV.

II. VACUUM BASELINE

A. Engineering the quark-initiated jet fraction

A key quantity in this paper is the quark-initiated jet fraction, q-fraction in short. We begin by analyzing its rapidity dependence on a dijet sample in $p + p$ collisions at LHC energies ($\sqrt{s} = 5.02$ TeV) using the PYTHIA [56] event generator. This quantity is defined as follows. First, we reconstruct anti-k_t [58] jets of radius $R = 0.4$ with FastJet [59]. The quark- or gluon-initiated tag is assigned according to a coincidence procedure, introduced in Ref. [20], and valid at leading order (LO): For a given jet, we find the parton produced by the hard-scattering matrix element whose angular distance $\Delta R \equiv \sqrt{\Delta\phi^2 + \Delta\eta^2}$ with respect to the jet axis is minimized. We then assign the quark- or gluon-initiated jet tag depending on the identity of the selected hard parton, considered to be the shower initiator. By selecting different jet momenta and rapidities, one effectively changes the value of Bjorken-x explored in the incoming protons, i.e., $x = 2p_t \cosh(y)/\sqrt{s}$, and, thus, the flavor of the parton that participates in the hard scattering. The quark-initiated jet fraction as a function of both the jet rapidity y and transverse momentum p_t is shown in the left panel in Fig. 1. We observe that the q-fraction is enhanced both at forward rapidities and at high jet p_t. This is expected, since at large values of x the parton distribution function (PDF) of valence quarks dominate. Thus, by selecting jets within a given p_t range and different bins in rapidity, we can engineer the q-fraction of a given jet ensemble.

As one moves toward larger rapidities, thereby approaching the kinematic limit determined by the center-of-mass energy of the hadronic collision, the jet p_t spectrum becomes increasingly steeper, as shown in the right panel in Fig. 1. These two rapidity-dependent properties of jets, namely, the evolution of the q-fraction and the evolution of the power index of the spectrum, n, are the two determining factors to understand jet suppression, or $R_{\rm AA}$, as a function of rapidity, as will be discussed in Sec. III B.

Using the spectra from the right panel in Fig. 1, we can estimate the expected number of jets in the HL-LHC corresponding to a range of q-fraction values for different windows in jet p_t and y.[7] The number of jets is simply given by $N_{\rm jets}(\Delta p_t, \Delta y) \approx \mathcal{L} N_{\rm coll} \int_{\Delta p_t, \Delta y} d\sigma/dp_t dy$, and we set $\mathcal{L} = 10$ nb^{-1} and $N_{\rm coll} \approx 2000$ for central collisions. The results are shown in Table I. As we will explicitly see when computing medium modifications in Secs. III B and III C, these numbers guarantee enough statistics to disentangle the physical mechanisms under consideration in the present work.

B. Analytic results at double-logarithmic accuracy

Next, we focus on the k_t distribution of the *hardest* splitting in the jet clustering sequence, as defined by the dynamical grooming procedure [60] with $a = 1$.[8] We use

[7]The actual center-of-mass energies will be $\sqrt{s} = 5.5$ ATeV, so we expect a slightly larger number of jets than the ones we estimate by using the spectrum at $\sqrt{s} = 5.02$ ATeV.

[8]Since we are measuring the k_t distribution of the splitting with the highest k_t, the groomed distribution is equivalent to the plain one.

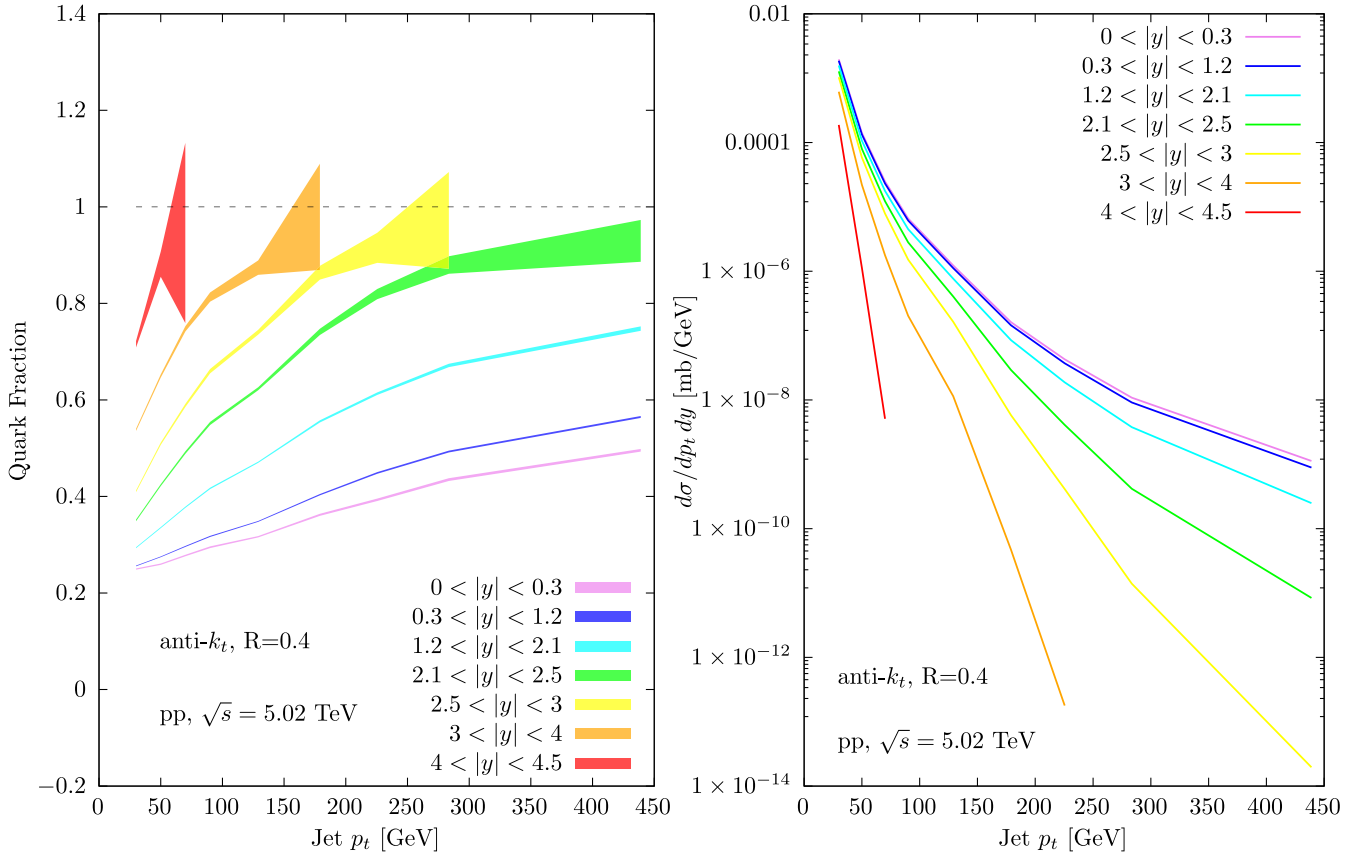

FIG. 1. Left: quark-initiated jet fraction as a function of the jet p_t for different intervals of jet rapidity y. Right: the same as the left panel but for the inclusive jet spectrum.

the small-angle approximation and define $k_t = z\theta$, where z and θ are the momentum sharing fraction and opening angle of the splitting, respectively. This observable was calculated at next-to-next-to-double-logarithmic accuracy and compared to ALICE data in Refs. [61,62]. In the present analytic study, we do not aim at providing precise predictions but rather focus on qualitative features of the distribution. As such, we consider all emissions to be soft and collinear. At this double-logarithmic accuracy (DLA) the self-normalized k_t distribution is given by

TABLE I. Estimated number of jets, N_{jets}, to be measured in heavy-ion collisions in the high-luminosity phase of the LHC for a given q-fraction range depending on the jet p_t. Guiding us with the left panel in Fig. 1, we select the following rapidity windows. For q-fraction $\lesssim$0.3, all jet p_t bins use the window $|y| < 0.3$. For q-fraction $\lesssim$0.6, low p_t uses $2.5 < |y| < 3$, mid p_t uses $2.1 < |y| < 2.5$, and high p_t uses $1.2 < |y| < 2.1$. Finally, for q-fraction $\lesssim$0.9, low p_t uses $4 < |y| < 4.5$, mid p_t uses $3 < |y| < 4$, and high p_t uses $2.1 < |y| < 2.5$.

Number of jets			
	q-fraction		
Jet p_t	$\lesssim$0.3	$\lesssim$0.6	$\lesssim$0.9
$20 < p_t < 80$ GeV	3.2×10^8	2.7×10^8	1×10^7
$100 < p_t < 150$ GeV	8×10^5	4×10^5	5.4×10^4
$225 < p_t < 300$ GeV	1.6×10^4	3.4×10^4	1.5×10^3

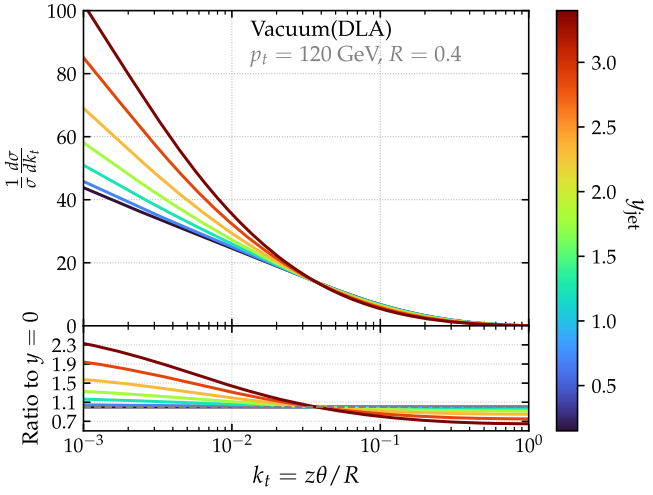

FIG. 2. Leading-k_t distribution as a function of rapidity in vacuum at DLA for jets with $p_t = 120$ GeV and $R = 0.4$. The bottom panel display the ratio to the midrapidity result.

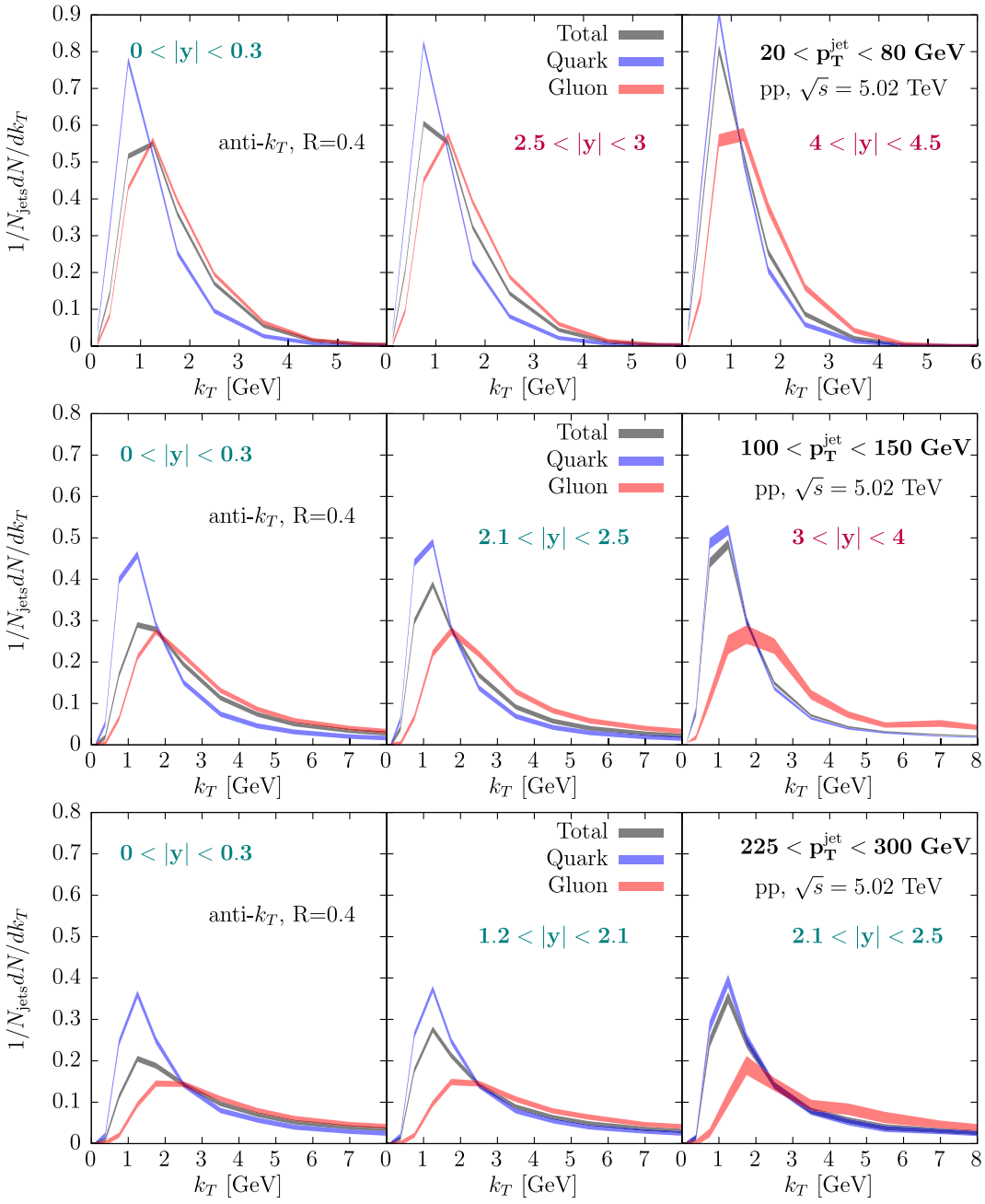

FIG. 3. Leading-k_t distribution for quark-initiated and gluon-initiated jets, as well as the total result, where each panel selects jets with different rapidity cuts that tag different q-fractions, as specified by Table I. From top to bottom, the jet p_t increases. The p_t and rapidity cuts that are accessible with the current LHC technology are marked in teal, while those of the future LHC runs are highlighted in purple.

$$\left.\frac{1}{\sigma}\frac{\mathrm{d}\sigma}{\mathrm{d}k_t}\right|_{p_t,y} = \sum_{i\in\{q,g\}} f_i \int_0^1 \mathrm{d}z \int_0^R \mathrm{d}\theta\, P^{\mathrm{vac}}(z,\theta)\delta(k_t - z\theta) e^{-\int \mathrm{d}z' \int \mathrm{d}\theta' P^{\mathrm{vac}}(z',\theta')\Theta(z'\theta' - k_t)}$$
$$\overset{\mathrm{DLA}}{=} \sum_{i\in\{q,g\}} f_i \frac{2\bar{\alpha}}{k_t} \ln\frac{R}{k_t} e^{-\bar{\alpha}\ln^2\frac{R}{k_t}}, \tag{1}$$

where we fixed the strong coupling to $\bar{\alpha} \equiv \alpha_s(p_t R) C_i/\pi$ with C_i the color factor, f_i corresponds to the quark (or gluon) fraction, and we have used that the branching kernel reduces to $P^{\mathrm{vac}} = \bar{\alpha}/(z\theta)$ in the soft-and-collinear limit.

In Fig. 2, we plot Eq. (1) for different rapidities.[9] We observe that the low-k_t regime is enhanced with increasing rapidity due to the more collimated DGLAP evolution of q-initiated jets. Note that, at this level of accuracy, the maximum of the distribution is dictated by the strong coupling constant, i.e., $k_{t,\max} \propto e^{-1/(2\bar{\alpha})}$ [61]. We cut the plot at $z\theta/R = 10^{-3}$ to downplay the region where nonperturbative corrections would dominate.

C. PYTHIA results

Since the previous calculation misses several ingredients of a realistic parton shower, we also calculate the leading-k_t distribution using PYTHIA simulations. The results are shown in Fig. 3 for quark- and gluon-initiated jets, as well as the total result. We reconstruct the particles of an anti-k_t jet with $R = 0.4$ using the Cambridge/Aachen algorithm [63] and look for the highest k_t throughout its clustering history, starting from the last clustering and following the leading branch. Note that for this particular figure we use a definition of k_t with dimensions of energy, $k_t \equiv z p_t^{\text{parent}} \sin\theta$, where p_t^{parent} is the momentum of the parent branch. In consistency with what is shown in Fig. 1, the inclusive results for leading k_t almost coincide with the gluon results at midrapidity, while they are dominated by the quark results when increasing the jet p_t and/or selecting larger rapidities. As expected from the analytics (see Fig. 2), the k_t distribution for quark-initiated jets is shifted toward smaller values compared to that of gluon-initiated jets.

III. MEDIUM RESULTS

In the previous section, we gained intuition on the shape of the leading-k_t distribution for quark- and gluon-initiated jets and how we can engineer jet samples with different q-fractions by selecting jets that belong to specific p_t ranges and rapidity windows. We now move to the description of the medium effects on this observable. Our main goal is to study how the different physical descriptions of the jet-medium interaction (modified q/g fraction and color decoherence) provide distinctive results as we study the medium modifications of jet ensembles with different q-fractions.

A. Analytic calculation in the multiple, soft scattering approximation

Let us begin by generalizing Eq. (1) to include medium modifications following the approximations introduced in Ref. [57]. The medium-modified leading-k_t distribution is given by

$$\left.\frac{1}{\sigma}\frac{\mathrm{d}\sigma}{\mathrm{d}k_t}\right|_{p_t,y} = \frac{1}{\mathcal{N}}\sum_{i\in\{q,g\}} f_i^{\mathrm{n}} \int_0^1 \mathrm{d}z \int_0^R \mathrm{d}\theta\, P_i^{\mathrm{med}}(z,\theta) \times \mathrm{e}^{-\int \mathrm{d}z' \int \mathrm{d}\theta' P^{\mathrm{med}}(z',\theta')\Theta(z'\theta'-k_t)} \delta(k_t - z\theta) \times \int_0^\infty \mathrm{d}\varepsilon \mathcal{E}_i(\varepsilon|z,\theta)\mathrm{e}^{-\frac{n\varepsilon}{p_t}}, \tag{2}$$

where $\mathcal{N}$ is a normalization factor, f_i^{n} is the quark or gluon fraction computed using nuclear PDFs (NPDFs), and n is the spectral index of the p_t spectrum.[10] The two main novelties of Eq. (2) are the in-medium branching kernel P^{med} and the energy loss probability distribution $\mathcal{E}$. The former accounts for the fact that the tagged emission can be either vacuumlike or medium induced and may include constraints on the radiation phase space. The latter represents the probability for an i-initiated splitting to radiate energy ε out of the jet cone via a medium-induced cascade.

In what follows, we will specify the exact form of P^{med} and $\mathcal{E}$ in two different models: the modified q/g modification model and another based on color decoherence. We emphasize that we make numerous approximations to simplify the models as much as possible while maintaining their main physical ingredients. Consequently, the following results serve an illustrative purpose and are not meant to be quantitative predictions. For the color decoherence-based model, we follow Ref. [57] and consider the QGP to be a brick of length $L = 4$ fm characterized by the transport coefficient $\hat{q} = 0.3\ \mathrm{GeV}^3$ and a coupling constant for medium-induced emissions of $\alpha_s^{\mathrm{med}} = 0.24$. These values lead to a reasonably good description of the jet yield depletion defined as

$$R_{\mathrm{AA}} = \frac{\mathrm{d}\sigma^{AA}/\mathrm{d}p_t}{\mathrm{d}\sigma^{pp}/\mathrm{d}p_t}, \tag{3}$$

in heavy-ion collisions, i.e., $R_{\mathrm{AA}} \sim 0.47$ at $p_t = 120$ GeV and $R = 0.4$. Keeping the same parameters for the modified q/g fraction model would lead to a different value of R_{AA}, since the energy loss model is different. Imposing that R_{AA} coincides in both models at $p_t = 120$ GeV leads to $L = 4$ fm, $\hat{q} = 0.7\ \mathrm{GeV}^3$, and $\alpha_s^{\mathrm{med}} = 0.28$.[11]

We remark that we keep L fixed for all rapidity values. To understand why this is correct, let us consider a particle moving perpendicular to the beam axis that travels a length x. If instead the particle moves with some longitudinal

[9] Our analytic results, both in vacuum and in the medium, rely, in general, on the properties of the species- and rapidity-dependent initial jet spectra, such as their power index n and q-fraction. We have used PYTHIA results to perform a fit of the jet p_t spectra, for jet-initiator species k within a rapidity window y, as $\mathrm{d}\hat{\sigma}^{(k,y)}/\mathrm{d}p_t = \sigma_0^{(k,y)}(p_{t,0}^{(k,y)}/p_t)^{n^{(k,y)}(p_t)}$ and $n^{(k,y)}(p_t) = \sum_{i=0}^{2} c_i^{(k,y)} \ln^i(p_{t,0}^{(k,y)}/p_t)$.

[10] Similarly to the vacuum case, we have performed a fit to the jet spectra $\mathrm{d}\sigma^{(k,y)}/\mathrm{d}p_t$, with the only difference being the use of the central set of the NPDFs provided by Eskola, Paakkinen, Paukkunen, and Salgado (EPPS16) [64].

[11] Many other combinations of $(L, \hat{q}, \alpha_s^{\mathrm{med}})$ would yield the same R_{AA}.

momentum, it will traverse, in the center-of-mass frame, a length $x' = x/\cos\theta$, where θ is the angle with respect to the direction perpendicular to the beam. Using the definition of rapidity, $y \equiv \text{arctanh}(p_z/p)$, with p_z and p being the longitudinal momentum and total momentum of the particle, respectively, one sees that $\cos\theta = 1/\cosh y$, so we can express the length traveled by the particle with a finite rapidity in the center-of-mass frame as $x' = x\cosh y$. Now, the quantity that matters for energy loss is the distanced traveled by a particle in the local fluid rest frame (LFRF). In general, the collision center-of-mass frame will not coincide with the LFRF, and so a Lorentz transformation needs to be performed to translate x' into its LFRF analog, that we denote x'_F. For the case in which a parton is moving with rapidity y and some transverse velocity through a Bjorken flow, one gets that $x'_F(y) = x'/\cosh y$ (see, e.g., Ref. [65]). Then, after taking this factor into account, we obtain that $x'_F = x$. That is, regardless of the rapidity of the particle, it will always traverse a length x in the LFRF, as if it was moving transversely to the beam axis. This justifies the use of a rapidity-independent medium length L.[12]

1. Modified q/g fraction model

We consider a description of the in-medium jet evolution that resembles the one presented in Refs. [20,21]. To start with, the branching kernel is taken to be the vacuum one; i.e., the leading-k_t condition is always met by a vacuum emission, and, therefore, we set $P^{\text{med}} \to \bar{\alpha}/(z\theta)$ in Eq. (2). Regarding the energy loss distribution, we assume that the intrajet activity is irrelevant, and, thus, every jet loses energy as if it was a single color charge. That is, we follow the quenching weights paradigm [67] and calculate the probability for a single parton of flavor i to lose energy ϵ as

$$\mathcal{Q}_i(p_t,R) \equiv \int_0^\infty d\epsilon \mathcal{E}_i(\epsilon|z,\theta) e^{-\frac{n\epsilon}{p_t}} = \exp\left[\int_R^\infty d\theta \int_0^1 dz P_i^{\text{mie}}(z,\theta)(e^{-nz}-1)\right], \quad (4)$$

where we adopt the multiple, soft scattering approximation to describe the spectrum of medium-induced emissions, i.e.,

$$P^{\text{mie}}(z,\theta) = \bar{\alpha}_{s,\text{med}}\sqrt{\frac{2\omega_c}{z^3 p_t}}\Theta(\omega_c - z p_t) \times 2\theta\frac{z^2 p_t^2}{Q_s^2}\Gamma\left(0, \frac{z^2 p_t^2 \theta^2}{Q_s^2}\right), \quad (5)$$

[12]The initial energy density profile in rapidity typically presents a plateau up to $|y| \approx 3$, followed by a Gaussian falloff that leads to a reduction of a factor 0.5 at around $|y| \approx 4.5$ [66]. This means that the medium is actually less hot and dense at these higher rapidities, leading to a reduction of L. While considering smaller L would affect the overall size of quenching for all jets, it does not alter the conclusions of this work.

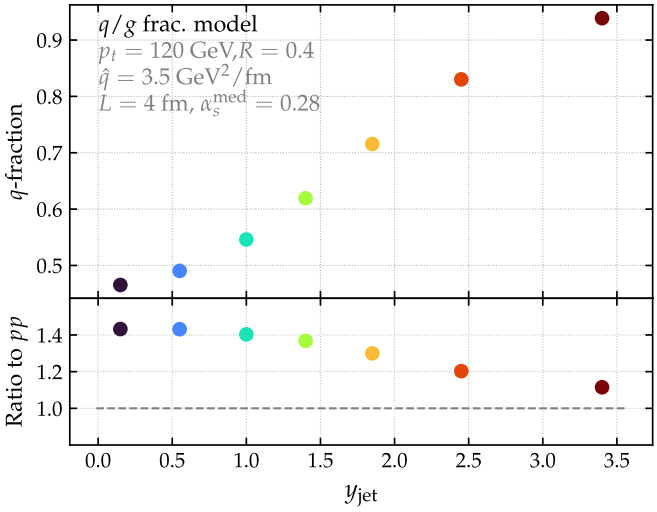

FIG. 4. Quark fraction as a function of rapidity for jets with $p_t = 120$ GeV calculated in the modified q/g fraction model. The bottom panel display the ratio to the $p+p$ result.

with $\omega_c = \hat{q}L^2/2$ being the maximum frequency that a medium-induced emission can acquire and $Q_s = \sqrt{\hat{q}L}$ its typical transverse momentum. The first line in Eq. (5) corresponds to the energy spectrum, while the second line describes transverse momentum broadening. Note that Eq. (5) is an approximation of the fully differential medium-induced spectrum that is valid only in the $k_t \ll Q_s$ and $\omega \ll \omega_c$ limit, i.e., in the soft-and-collinear limit.

Having specified the ingredients of the model, an important remark is in order. The shape of the energy loss distribution impacts the q/g fraction of the jet sample after quenching.[13] An important aspect of Eq. (4) is that our energy loss model follows Casimir scaling. In this sense, it is similar to that of Ref. [20], but it is expected to differ from Ref. [21]. The q-fractions obtained with our toy model are displayed in Fig. 4. At midrapidity, our q-fraction, driven by a Casimir scaling of energy loss, is similar to that of Ref. [24] but substantially lower than that of Ref. [21]. This implies that our results for the k_t distribution correspond to a conservative version of the modified q/g fraction model. We will explore q-fraction values similar to those of Ref. [21] using Monte Carlo simulations in Sec. III C. The evolution with rapidity of the ratio of the q-fraction between Pb + Pb and $p+p$ is displayed in the lower panel in Fig. 4. This marked evolution, getting close to no modification at all at forward rapidities, compactly elucidates the motivations of the proposed rapidity scan.

In Fig. 5, we show results for the coherent modification of the leading-k_t distribution as a function of the jet rapidity and take the ratio with respect to the vacuum baseline.

[13]The q-fraction can be obtained by fixing the flavor in Eq. (2), integrating over k_t, and dividing by the total jet cross section $\mathcal{N}$.

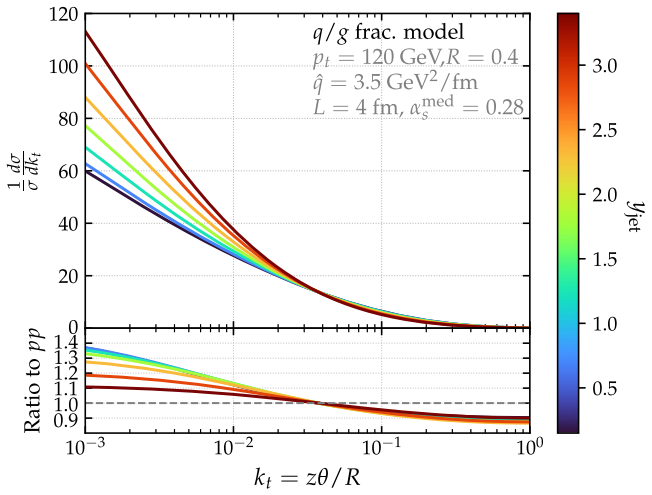

FIG. 5. Leading-k_t distribution in the medium using the modified q/g model for jets with $p_t = 120$ GeV. The bottom panel displays the ratio to the $p + p$ result.

Attending to the message provided by Fig. 4, the interpretation of these results is quite transparent: The visible narrowing of the k_t distribution at midrapidities is greatly reduced when the q-fraction is so high that the depletion of gluon jets in the measured Pb + Pb ensemble becomes irrelevant. Naturally, this model predicts a ratio of the k_t distribution with respect to $p + p$ close to one at large rapidities. Note that, if following Ref. [21] and one started with a larger value of the q-fraction in Pb + Pb at midrapidity, the approach of the k_t distribution toward the vacuum result with increasing rapidities would be more abrupt.

2. Color decoherence model

We now turn to a theoretical description of the leading-k_t distribution based on Ref. [57]. Here, we give a brief summary of the main ingredients of the model, while a more detailed description can be found in Ref. [57]. This calculation, grounded in perturbative QCD, accounts for the factorization in time between vacuumlike and medium-induced processes in the double-logarithmic approximation. In this case, the medium branching kernel reads

$$P^{\mathrm{med}}(z,\theta) = P^{\mathrm{vac}}(z,\theta)\Theta_{\notin \mathrm{veto}}(z,\theta) + P^{\mathrm{mie}}(z,\theta), \quad (6)$$

where $\Theta_{\notin \mathrm{veto}}$ constrains the phase space for vacuumlike emissions to be [39]

$$\Theta_{\notin \mathrm{veto}}(z,\theta) = 1 - \Theta(\theta - \theta_c)\Theta(k_t^2 - k_{t,\mathrm{med}}^2)\Theta(L - t_f), \quad (7)$$

with the formation time of an emission given by $t_f = 2/(k_t\theta)$ and $k_{t,\mathrm{med}}^2 = \hat{q}t_f$ is the minimum transverse momentum acquired by the emission via multiple soft collisions during its formation. In a nutshell, Eq. (7) imposes that vacuum emissions inside the medium are allowed only for sufficiently high values of k_t or, equivalently, short formation times such that they are not affected by medium dynamics. This separation has been rigorously proven at DLA in Ref. [39].

Note that compared to the model presented in Sec. III A 1, Eq. (6) includes two new ingredients: (i) the possibility that a medium-induced emission is the one with the highest k_t and (ii) a restriction in the phase space for vacuum emissions. Regarding the first point, since we describe the interactions between the hard propagating parton and the medium in the multiple, soft scattering approximation, we use Eq. (5) to describe the medium-induced branching probability. This is an important aspect of the calculation, since the leading-k_t distribution has been proposed as a potential observable to search for QCD Molière scattering in the medium [68–70]. Importantly, our analytic estimates provide the multiple, soft scattering baseline for future studies which will account for rare, hard scatterings. Note that the transverse diffusion term in Eq. (5) can lead to a broadening of the k_t distribution.

The calculation of the energy loss probability distribution in this model reduces the whole jet to just the tagged splitting. Then, depending on whether the angle of the splitting is smaller or larger than the QGP resolution angle θ_c, the jet will lose less or more energy. That is, we replace the last line in Eq. (2) with

$$\int_0^\infty d\varepsilon \mathcal{E}_i(\varepsilon|z,\theta)e^{-\frac{n\varepsilon}{p_t}} = (1 - \Theta_{\mathrm{res}})\mathcal{Q}_i(p_t,R) + \Theta_{\mathrm{res}}\mathcal{Q}_g(p_t,R)\mathcal{Q}_i(p_t,R), \quad (8)$$

where the resolution criterion reads

$$\Theta_{\mathrm{res}}(z,\theta) = \Theta(\theta - \theta_c)\Theta(k_t - k_{t,\mathrm{med}}). \quad (9)$$

The physical meaning of Eq. (8) is rather simple. The first term accounts for the case in which the splitting is unresolved, and, thus, the jet loses energy as a global color charge, just like in the modified q/g fraction model. In turn, the second term in Eq. (8) describes the energy loss of a splitting resolved by the medium as the product of the quenching weight of both prongs. We emphasize that this model is a rather crude simplification of the dynamics of color coherence. We plan to explore the use of a resummed quenching weight [71] for jet substructure calculations together with a determination of the phase space for vacuumlike emissions beyond the double-logarithmic approximation in a separate publication [72].

The leading-k_t distribution for this model is displayed in Fig. 6. We observe a drastically different result compared to Fig. 5: Medium modifications on the k_t distribution are enhanced at forward rapidities. In fact, we observe, for all rapidities, an enhancement of k_t values around the scale $\theta_c/(2R)$, that is, when the energy is shared democratically

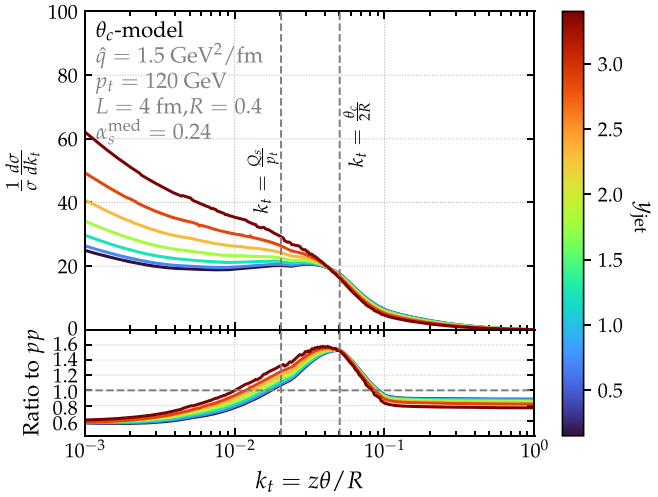

FIG. 6. Leading-k_t distribution in the medium using the color decoherence model for jets with $p_t = 120$ GeV. The bottom panel displays the ratio to the $p + p$ result. We have highlighted two particularly relevant scales that are further discussed in the main text.

between the two prongs and the opening angle is identical to the critical one. The only scale in this model is θ_c, and it is, thus, natural that the k_t distribution exhibits a great sensitivity to it, as was also the case in the study performed in Ref. [57] for the opening angle of the splitting. We also observe that this enhancement at $k_t = \theta_c/(2R)$ is more pronounced at forward rapidities. In this plot, we have highlighted as well the typical scale for medium-induced emissions, i.e., $k_t = Q_s/p_t$.

Let us now focus on the rapidity dependence of this model. At asymptotically large rapidities, quarks dominate the sample, and the quenching weight corresponding to the emitter in Eq. (8) always reduces to that of a quark. All those splittings with $\theta > \theta_c$ are resolved and, therefore, suppressed, leading to an enhancement of the relative yield of jets featuring small-k_t (equivalently, small-angle) splittings. This filtering mechanism becomes less effective at midrapidity, since there one has an admixture of quarks and gluons. The fact that the sample is not pure is important, since energy loss depends on both the color factor and the opening angle of the splitting. Because of their vacuumlike evolution, gluon-initiated jets are on average broader than quark-initiated jets, so it is more likely that they can be resolved by the medium. However, gluon-initiated jets with unresolved, small-k_t splittings can be more quenched than quark-initiated ones, since $\mathcal{Q}_g \propto \mathcal{Q}_q^{C_A/C_F}$. The competition between these two effects, i.e., the color charge and the opening angle of the splitting, yields an overall milder narrowing at midrapidity than in the forward regime.

To sum up this analytic section, we have identified an experimental measurement that could pin down the origin of the narrowing effect observed for midrapidity jets. These analytic estimates have allowed us to highlight the core ideas underlying the potential of jet substructure measurements at forward rapidities to disentangle between different jet quenching dynamics. In what follows, we turn to a more quantitative approach and present predictions both with the hybrid Monte Carlo model and with a modified q/g fraction model that uses PYTHIA as its vacuum baseline.

B. The hybrid strong-weak coupling model

The hybrid strong-weak coupling model [41,65] combines a perturbative high-Q^2 evolution of the parton shower[14] together with a nonperturbative description of the dynamics between the jet partons and the strongly coupled QGP. The amount of hydrodynamized energy per unit length has been computed in a strongly coupled $\mathcal{N} = 4$ super Yang-Mills plasma at large-N_c and infinite coupling [74,75]:

$$\left.\frac{\mathrm{d}E}{\mathrm{d}x}\right|_{\text{strongly coupled}} = -\frac{4}{\pi}E_{\mathrm{in}}\frac{x^2}{x_{\mathrm{stop}}^2}\frac{1}{\sqrt{x_{\mathrm{stop}}^2 - x^2}}, \quad (10)$$

where $x_{\mathrm{stop}} \equiv E_{\mathrm{in}}^{1/3}/(2T^{4/3}\kappa_{\mathrm{sc}})$ is the distance an energetic parton with initial energy E_{in} will travel within the strongly coupled medium before completely hydrodynamizing. κ_{sc} is an $\mathcal{O}(1)$ parameter fitted to hadron and jet heavy-ion data measured at the LHC [76]. The energy and momentum lost by the colored charges [cf. Eq. (10)] hydrodynamize and excite a wake in the flowing plasma, described hydrodynamically, which later decays into soft hadrons at the freeze-out hypersurface. We estimate the distributions of those hadrons by applying the Cooper-Frye prescription to the jet-induced perturbations, where we assume that the background fluid is characterized by Bjorken flow and that the perturbations stay close in rapidity around the jet [77]. Improvements to this approximated description of medium response are in development [78].

All results in this work will include the wake, and comparisons against the results without the wake will not be presented. Even though the wake has an important effect for jets with larger cones [79–82], its impact on moderate $R \sim 0.4$ cones is milder and does not play an important role for the kind of jet ensembles here considered. The effect of the soft hadrons from the wake on jet substructure, for inclusive jet ensembles at high enough jet p_t, is also subleading, due to a selection bias effect [43,83] in which the narrower, less quenched jets, which naturally have associated a smaller wake, represent a large fraction of the

[14]The perturbative evolution includes initial-state radiation (ISR), although, due to both grooming and the small cone size considered in this work, its impact is negligible. We refer the reader to Ref. [73] for a recent study of ISR on jet substructure observables in heavy-ion collisions.

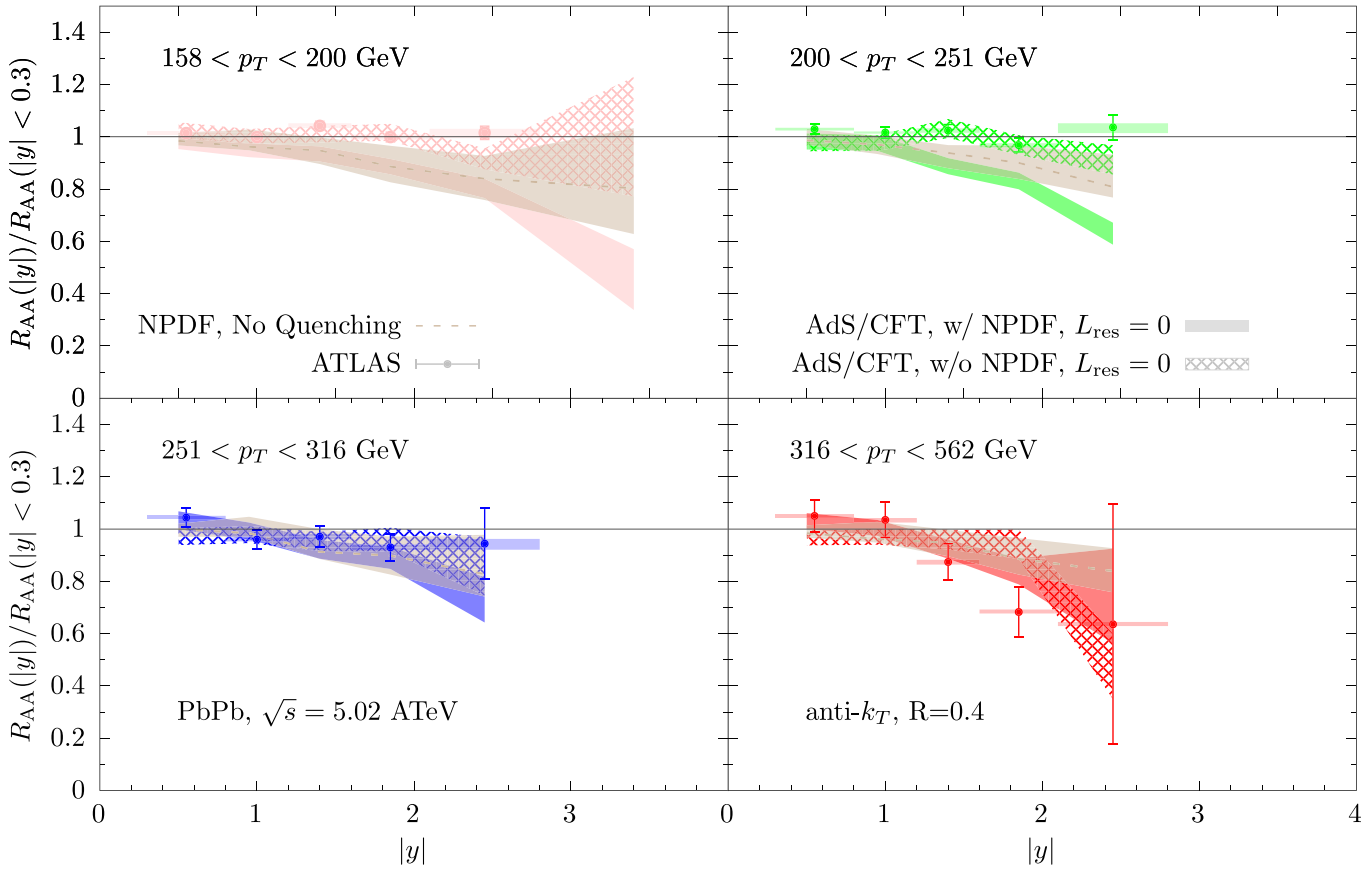

FIG. 7. $R_{\rm AA}$ ratio between results at a given rapidity $|y|$ and those at midrapidity ($|y| < 0.3$). Jets are reconstructed with anti-k_t and $R = 0.4$. Results are shown for different jet p_t bins.

measured jet population after imposing p_t cuts [84].[15] Note that alternative descriptions of medium response in which the recoils from the elastic scattering processes stay relatively close to the jet axis can present more sizable effects on, e.g., groomed observables of inclusive jet samples [87].

Finite resolution effects are incorporated in the hybrid model [42] in analogy to the notion of screening: The resolution length $L_{\rm res}$ determines the minimal distance between two color charges such that they engage with the QGP independently. We will mainly focus in two limiting regimes: (i) $L_{\rm res} = 0$, when partons are resolved the instant after they are formed, and (ii) $L_{\rm res} = \infty$, that corresponds to the fully unresolved scenario in which the QGP is sensitive to the global color charge of the jet only. Compared to our analytic results from the previous section, $L_{\rm res} = \infty$ resembles the coherent energy loss implemented for the modified q/g fraction model, while a finite value of $L_{\rm res}$ (that will also be explored) would play the role of θ_c in the color decoherence model.

[15]The effect of the wake on jet substructure observables can be enhanced by selecting very quenched jets using boson-jet samples [85] or machine learning techniques [86].

In view of the goals of the present study, the distinctive color-charge dependence of energy loss in this model deserves some comment. Within an holographic energy loss scenario, the different quenching between quarks and gluons scales like $\mathcal{C} \equiv (C_A/C_F)^{1/3} \simeq 2^{1/3}$ at large N_c [88], in contrast to the linear C_A/C_F scaling expected from perturbative arguments. Since the energy loss rate Eq. (10) was derived for the dual of a parton in the fundamental representation, a quark, this means that $\kappa_{\rm sc}^G = \kappa_{\rm sc}\mathcal{C}$. Therefore, the pure q/g fraction effect is by construction milder than in perturbative QCD (pQCD)-inspired energy loss scenarios. However, when the traversed distance is much smaller than the stopping distance, i.e., $\epsilon \equiv x/x_{\rm stop} \ll 1$, the energy loss rate Eq. (10) can be expanded in powers of ϵ and, to leading order, the dependence on the Casimirs becomes linear, as in pQCD. Deviations from the full expression start to become significant [$\mathcal{O}(10\%)$] at around $\epsilon \approx 0.7$, which for a $T = 0.25$ GeV and a traversed length of $x = 5$ fm means that, for partons with $E_{\rm in} > 100$ GeV, the color charge dependence is well described by a linear Casimir scaling.

Before moving on to analyze the modification of the leading-k_t distribution with the hybrid model, and especially its rapidity dependence, it is important to understand

whether the rapidity dependence of jet suppression itself is reasonably described.

1. Rapidity dependence of jet suppression

The energy loss rate in Eq. (10) was actually derived for a parton moving through a fluid in the local fluid rest frame. Following the discussion by the end of the introduction to Sec. III A, given that the QGP is well approximated as a Bjorken flow, energy loss of a given single parton using Eq. (10) is, in practice, very mildly dependent on rapidity. Therefore, any rapidity dependence of jet suppression found in observables has to have its origin elsewhere.

In Fig. 7, we show results for jet suppression, for different cuts in rapidity using $L_{\rm res} = 0$ (using $L_{\rm res} = \infty$ yields a very similar picture). We present the results as ratios to the $|y| < 0.3$ result for different jet p_t bins and compare against ATLAS data [8]. In addition, we calculate this observable with and without nuclear PDFs using the EPPS16 [64] set. We discuss the results without NPDFs first. As the quark fraction increases with rapidity (cf. left panel in Fig. 1), so does $R_{\rm AA}$, meaning less suppression, as quark jets tend to be less quenched. On the other hand, by increasing rapidity, the initial jet spectrum becomes steeper, specially at higher jet p_t (cf. right panel in Fig. 1), which translates into a reduction of $R_{\rm AA}$. These competing effects yield an evolution of $R_{\rm AA}$ that is almost independent of rapidity within $|y| \leq 2$ (as was also observed in Refs. [20,89]). For very large rapidities, where one is approaching the kinematic limit at increasingly lower jet p_t, the steepness of the spectrum is the dominant effect, notably reducing $R_{\rm AA}$. Overall, there is good agreement between the hybrid model without NPDFs and the experimental data.

In turn, the results of the hybrid model with the inclusion of NPDFs (using only the central set for computing time reasons) are quite different. The initial-state-induced modification of the initial jet spectrum at moderate rapidities yields a reduction of $R_{\rm AA}$ with respect to midrapidity that is notable for a wide range in jet p_t. To highlight the sizable effect of the initial state on this observable, we show in a dotted bisque-colored line the results that use NPDFs but without quenching. For this "no quenching" baseline, we have also included the uncertainties associated to the 40 error sets, as prescribed in Ref. [64]. We can appreciate how the deviation from unity of the full results with NPDFs are actually dominated by the initial-state effects themselves, resulting into deviations from data in the first two p_t bins displayed in the top panels in Fig. 7. While the results in the second-to-highest jet p_t bin, in the bottom left panel, are the least sensitive to initial-state effects, the highest jet p_t bin, in the bottom right panel, indicates that data seem to slightly prefer those that include NPDFs. For this jet p_t bin, both NPDFs and quenching effects are needed to achieve the best description of experimental data, as was also noted in Ref. [90]. We have checked that initial-state effects reduce the q-fraction by less than 5% for low-p_t jets ($p_t < 80$ GeV) and have a negligible impact for higher jet pt. Therefore, we conclude that the observed impact of initial-state effects on the results in Fig. 7 is due to the modification of the underlying p_t spectrum. Clearly, future precision studies will also need to rely on background descriptions that account for the lack of longitudinal boost invariance toward larger rapidities, by using, for example, full $3+1$D hydrodynamical simulations. All in all, the results in Fig. 7 provide strong motivation to revisit the impact of initial-state effects in other jet quenching models.

Along with the previous observations on the sizable initial-state effects in jet $R_{\rm AA}$ at high p_t [80,91], which question the direct interpretation of $R_{\rm AA} \simeq 1$ as a signal of the recovery of lost energy for large-R jets [80], these results contribute to build a case for a thorough consideration of the role of NPDFs in jet quenching physics, especially in view of the future precision studies programmed at RHIC and the LHC. As a first step, it would be interesting to explore different PDF sets such as EPPS21 [92] or nNNPDF3.0 [93] and see whether this observable is capable of discriminating among different NPDF models.

2. Predictions for a rapidity scan of the leading-k_t distribution

In the previous section, we have demonstrated that the rapidity dependence of jet $R_{\rm AA}$ can be reasonably described by the hybrid model. We are now in a position to perform predictions on the rapidity dependence of jet substructure observables, such as the leading-k_t distribution. Before presenting our results for this observable, it is relevant to discuss the modification of the q-fraction due to medium effects in the hybrid model. We show in Fig. 8 the ratio between the q-fraction in Pb + Pb and in $p+p$ both for the fully resolved case, $L_{\rm res} = 0$, in solid bands, and for the fully unresolved case, $L_{\rm res} = \infty$, in grid pattern bands. In general, this ratio tends to decrease with increasing rapidities, as we saw in Fig. 4, because the value of the $p+p$ baseline in the denominator steadily increases.[16] There is an exception to this trend, observed in the different behavior for the results of the lowest jet p_t bin, in black. For jets with $20 < p_t < 80$ GeV, the ratio of the q-fraction can be somewhat larger for rapidity values around $|y| \gtrsim 2.5$ than the one at midrapidity. The reason for this is the strong jet p_t dependence in the value of the q-fraction for jets with $p_t \lesssim 100$ GeV at forward rapidities, as seen in the left panel in Fig. 1. Shifting the jet p_t has a notable effect on the value of the q-fraction at $|y| \approx 2.5$, while the impact is much smaller at midrapidity. Therefore, due to medium-induced energy loss, jet p_t bin migration leads to a sizable increase in the number of quark-initiated jets for those kinematic

[16]Discrepancies between the results in Figs. 4 and 8 are expected, since the energy loss model differs.

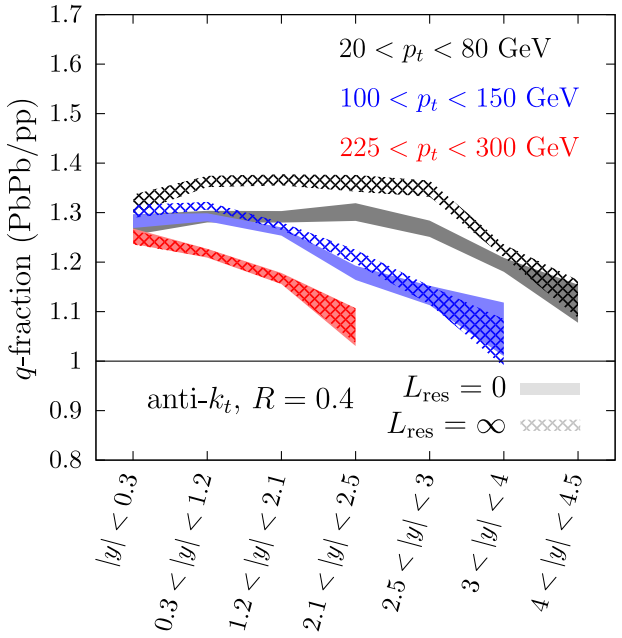

FIG. 8. Ratio of the q-fraction between Pb + Pb and $p + p$ for different jet p_t intervals and rapidity windows, comparing $L_{\mathrm{res}} = 0$ ($L_{\mathrm{res}} = \infty$) in solid (grid pattern) bands.

ranges in which the q-fraction features such a strong dependence with p_t.

In Fig. 8, we also observe that the scenario with $L_{\mathrm{res}} = \infty$ produces larger differences in the q-fraction between Pb + Pb and $p + p$. The differences with respect to the case with $L_{\mathrm{res}} = 0$ are approximately independent of the rapidity window and decrease in magnitude as jet p_t increases. We can understand this based on simple arguments. The ratio of the q-fraction can be expressed in terms of jet suppression as $f_q^{\mathrm{ratio}} \equiv R_{\mathrm{AA}}^q / R_{\mathrm{AA}}^{\mathrm{total}}$, this is, the suppression of quark-initiated jets divided by the total jet suppression. One can approximate $R_{\mathrm{AA}} \approx 1 - \varepsilon n / p_t$ [see Eq. (4)], where ε is the average energy lost per jet, n is the power index of the spectrum, and p_t is the jet transverse momentum. Then,

$$R_{\mathrm{AA}}^q \approx 1 - \varepsilon_q \frac{n}{p_t}, \tag{11}$$

$$R_{\mathrm{AA}}^{\mathrm{total}} \approx 1 - [\varepsilon_q f_q + \varepsilon_g (1 - f_q)] \frac{n}{p_t}, \tag{12}$$

where f_q represents the vacuum q-fraction and where we have assumed that quark and gluon jets have similar values of n. To leading power in $\varepsilon_i n / p_t$, we write

$$f_q^{\mathrm{ratio}} \approx 1 + (1 - f_q)(\varepsilon_g - \varepsilon_q) \frac{n}{p_t} + \mathcal{O}((\varepsilon n / p_t)^2). \tag{13}$$

In order to express the energy loss for a jet with a given flavor, we make use of the resummed quenching weights formalism in the small energy loss approximation [71]. In this limit, we can simply write

$$\varepsilon_q \sim C_F \hat{\varepsilon} [1 + C_A \mathcal{A}(p_t, R)], \tag{14}$$

$$\varepsilon_g \sim C_A \hat{\varepsilon} [1 + C_A \mathcal{A}(p_t, R)], \tag{15}$$

where $\mathcal{A}(p_t, R)$ refers to the phase space of extra energy loss sources (assumed to be all vacuumlike gluons) resolved by the medium and $\hat{\varepsilon}$ is now the average energy lost *per parton* (stripped of the color charge dependence). In the $L_{\mathrm{res}} = \infty$ case, the medium cannot resolve the phase space by definition, and so $\mathcal{A}_\infty \to 0$. Instead, when $L_{\mathrm{res}} = 0$, the medium resolves all emissions that are formed within the medium. At fixed coupling, $\mathcal{A}_0$ is, thus, given by

$$\begin{aligned} \mathcal{A}_0 &= \frac{\alpha_s}{\pi} \int \frac{\mathrm{d}z}{z} \int \frac{\mathrm{d}\theta}{\theta} \Theta(t_f < L) \Theta(\theta < R) \\ &= \frac{\alpha_s}{4\pi} \ln^2 \left(\frac{p_t R^2 L}{2} \right), \end{aligned} \tag{16}$$

where we have used $t_f = 2/(z\theta^2 p_t)$. Finally, we can obtain the difference in the q-fraction ratio between these two scenarios as

$$\begin{aligned} f_{q,\infty}^{\mathrm{ratio}} - f_{q,0}^{\mathrm{ratio}} \approx (1 - f_q) \frac{n}{p_t} (C_A - C_F) \\ \times \hat{\varepsilon}_\infty \left[1 - \frac{\hat{\varepsilon}_0}{\hat{\varepsilon}_\infty} (1 + C_A \mathcal{A}_0) \right]. \end{aligned} \tag{17}$$

Similarly to the fitting procedure adopted within the hybrid model, we impose a comparable $R_{\mathrm{AA}} \approx 0.5$ for both scenarios for jets with $p_t \approx 150$ GeV and $R = 0.4$. Using $L = 4$ fm, $f_q = 0.5$, $\alpha_s = 0.2$, and $n = 5$, we get that $\hat{\varepsilon}_\infty \approx 7$ GeV and $\hat{\varepsilon}_0 \approx 2.8$ GeV. By numerically evaluating Eq. (17), we obtain $\mathcal{O}(10\%)$ in the difference of f_q^{ratio} at $p_t \approx 80$ GeV, decreasing down to less than 2% at high jet p_t, around $p_t \approx 250$ GeV. These results are in qualitative agreement with what is observed in Fig. 8.

We discuss next the results of the medium-modified k_t distribution. In Fig. 9, we show the ratio between Pb + Pb and $p + p$ for the leading-k_t distribution, using the same cuts as in Fig. 3. For each of the individual plots, the main message is clearly the presence of a sizable narrowing of the leading-k_t distribution when the jet substructure can be resolved by the QGP, represented in this model by $L_{\mathrm{res}} = 0$ and $L_{\mathrm{res}} = 2/\pi T$. Note that the observed narrowing is notably stronger than the one obtained analytically in Fig. 6. This is most likely due to the fact that, as expressed in Eq. (8), quenching of a resolved jet simply consists in the energy loss from the two tagged prongs; there is no additional quenching for each of the possible subsequent emissions off these partons, as we do in the present Monte Carlo analysis. If one were to include the resummation of the quenching weights [71,82,94] in the analytic model, the quenching of the wider structures would be stronger, and the narrowing more pronounced. Another

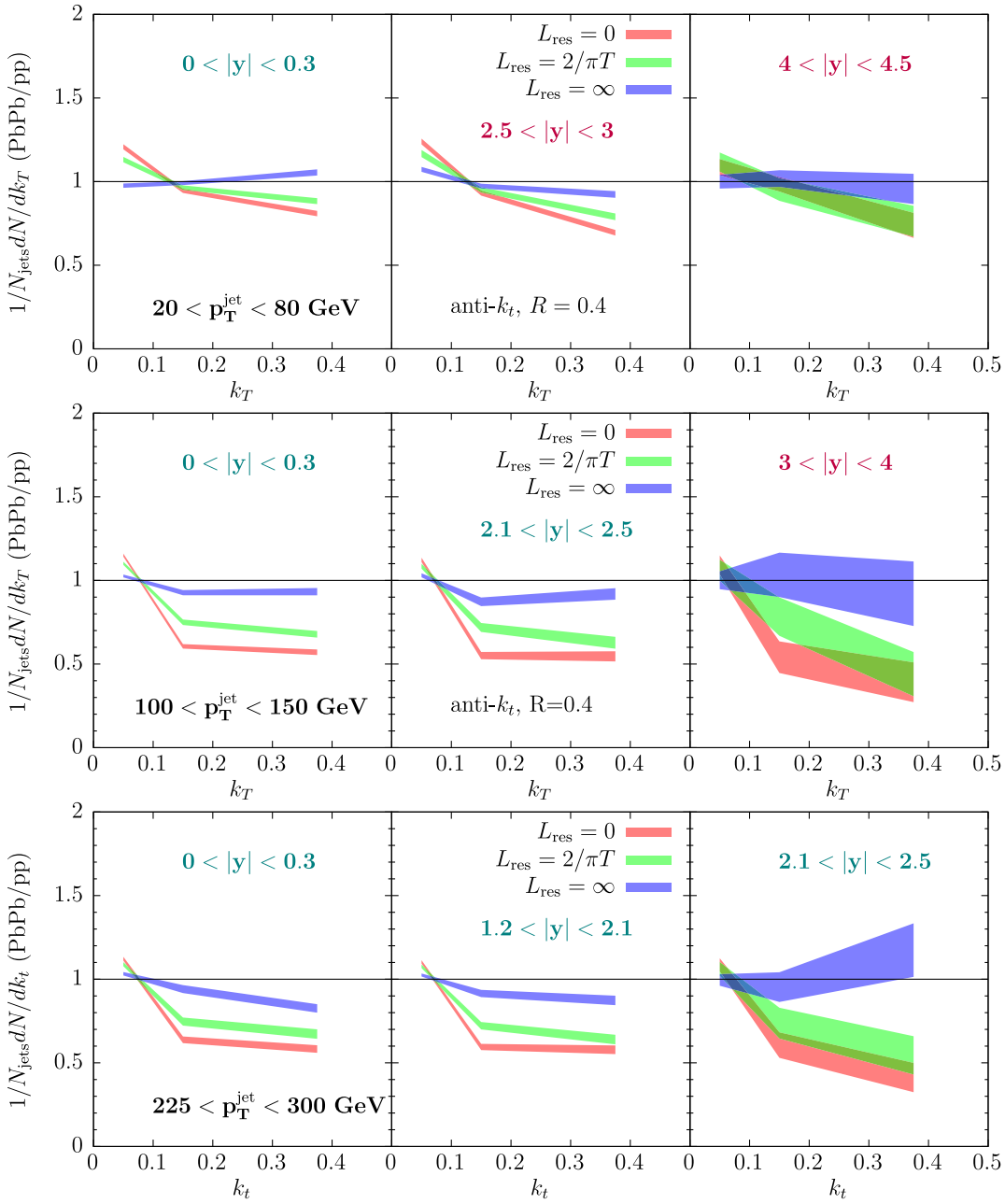

FIG. 9. Leading-k_t distribution calculated with the hybrid model for different rapidity and transverse momentum intervals. Note that we use a dimensionless expression for k_t, defined as $k_t \equiv z(p_t^{\rm parent}/p_t^{\rm jet}) \sin\theta/R$.

important remark is that the narrowing in the $L_{\rm res} = 0$ and $L_{\rm res} = 2/\pi T$ cases persists for all rapidities and that the differences between $L_{\rm res} = \infty$ and $L_{\rm res} = 0$ (or $L_{\rm res} = 2/\pi T$) are sufficiently large at the kinematic regions that already are experimentally accessible with current detector capabilities at the LHC. As expected, there is less narrowing for $L_{\rm res} = 2/\pi T$ than for $L_{\rm res} = 0$. However, the results for $L_{\rm res} = 2/\pi T$ are still closer to those with $L_{\rm res} = 0$ than to $L_{\rm res} = \infty$. Note that if $L_{\rm res} = 2/\pi T$ were to be translated to a "coherence angle," it would roughly correspond to (fixing $T = 0.3$ GeV and $L = 4$ fm, although, of course, both T and L fluctuate) $\theta_{\rm res} \approx 0.1$.

Focusing now on the $L_{\rm res} = \infty$ curves in Fig. 9, we can observe that the ratio becomes increasingly flat as we increase the vacuum q-fraction by moving toward larger rapidities. This is fully consistent with the picture obtained in Fig. 5. In addition, the evolution of this flattening becomes milder with decreasing jet p_t, since the q-fraction ratio does not evolve as strongly with rapidity, as we saw in Fig. 8. In the lowest jet p_t bin, there are a few interesting

features that we comment on. In this case, since the ratio of the q-fraction can actually increase (cf. Fig. 8), we find that the leading-k_t distribution is actually narrower for the $2.5 < |y| < 3$ bin than for the $|y| < 0.3$ bin. In fact, the mid-rapidity result is even slightly wider than in vacuum. We have checked that this last point is an effect of the wake, as the soft particles at large angles produced via jet-energy thermalization can contribute to generate, or enhance, structures sitting at the jet boundary.[17]

C. Modified q/g fraction model with PYTHIA templates

The goal of this section is to extend the analytic results presented in Sec. III A 1 by using as a vacuum baseline templates from PYTHIA with the estimated statistics of the future HL-LHC run. We do so as to realistically assess the feasibility of future experiments to pin down the differences between the results from a modified q/g fraction hypothesis and those obtained when the medium is capable of resolving the fluctuating substructure of each individual jet, i.e., $L_{\rm res} = 0$ and $L_{\rm res} = 2/\pi T$ results of the hybrid model presented in the previous section.

Our starting point consists in expressing $R_{\rm AA}$ in terms of the suppression experienced by quark- and gluon-initiated jets. The definition of jet suppression [Eq. (3)] can be recast into

$$R_{\rm AA} = f_q \mathcal{Q}_q + (1 - f_q)\mathcal{Q}_g, \tag{18}$$

where f_q is the quark-initiated jet fraction in vacuum and $\mathcal{Q}_q$ and $\mathcal{Q}_g$ are the (bare) quenching weights of quark-initiated and gluon-initiated jets, respectively. These bare quenching weights can be computed as in Eq. (4) within the Baier-Dokshitzer-Mueller-Peigne-Schiff and Zakharov approach. We can further use the fact that $\mathcal{Q}_i$ scales with the Casimir of the color charge exponentially [67], so that $\mathcal{Q}_g = \mathcal{Q}_q^{C_A/C_F}$. For the purposes of the present section, it is convenient to express Eq. (18) in terms of the relative suppression of gluon versus quark jets, $f_{\rm rel}$, as

$$\begin{aligned} R_{\rm AA} &= \mathcal{Q}_q[f_q + (1 - f_q)\mathcal{Q}_q^{C_A/C_F - 1}] \\ &= \mathcal{Q}_q[f_q + (1 - f_q)f_{\rm rel}]. \end{aligned} \tag{19}$$

Let us discuss a few meaningful values of $f_{\rm rel}$. To start with, choosing $f_{\rm rel} = \mathcal{Q}_q^{C_A/C_F - 1}$ corresponds to the relative suppression motivated by the Baier-Dokshitzer-Mueller-Peigne-Schiff and Zakharov physics encapsulated in Eq. (6), which for a reasonable value of $\mathcal{Q}_q = 0.6$ leads to $f_{\rm rel} \approx 0.5$, i.e., a factor of 2 increase in the relative number of quark jets over gluon jets, due to medium effects, when compared to vacuum. As mentioned in the introduction, the value $f_{\rm rel} = 0.25$ coincides with the one extracted via global fits to the jet fragmentation function [23] and used in further quenching studies of the modification of the groomed radius [15,21]. Finally, we also explore $f_{\rm rel} = 0.1$ to test the maximal effects from the modified q/g fraction hypothesis.

The medium-modified leading-k_t distribution, in close analogy to the formulas presented in Sec. III A 1, then reads

$$\frac{1}{\sigma}\frac{{\rm d}\sigma}{{\rm d}k_t}\bigg|_{AA} = \mathcal{N}^{-1}\left[f_q \frac{{\rm d}\sigma_q}{{\rm d}k_t}\bigg|_{pp} + f_{\rm rel}(1 - f_q)\frac{{\rm d}\sigma_g}{{\rm d}k_t}\bigg|_{pp}\right], \tag{20}$$

where $\mathcal{N} = f_q + f_{\rm rel}(1 - f_q)$. Note that the individual distributions are assumed to be unmodified with respect to vacuum. That is, they correspond to templates obtained using PYTHIA and shown in Fig. 3. An important caveat of Eq. (20) is that we keep $f_{\rm rel}$ fixed for all values of jet p_t and rapidity. As a consequence, this approach ignores the strong p_t dependence of the q-fraction for lower jet p_t at higher rapidities, as highlighted when discussing Fig. 8. This p_t dependence becomes important when spectra shifts, due to energy loss, modify the average jet p_t of a given jet ensemble. Keeping $f_{\rm rel}$ fixed also neglects any intrinsic p_t dependence of the substructure observable in consideration. Accounting for all these effects would require $f_{\rm rel} \to f_{\rm rel}(p_t, y)$.

In Fig. 10, we show results for the modification of the leading-k_t distribution using the toy model encapsulated in Eq. (20). They are presented as ratios with respect to the vacuum result, using the same kinematic cuts as in Figs. 3 and 9. The presence of the gray band responds to a sanity check that Eq. (20) reproduces the total vacuum result, $f_{\rm rel} = 1$, given the correct f_q. The values of f_q are estimated from Fig. 1 and then more finely tuned to get an exact ratio of 1. The statistics used for the Pb + Pb samples approximately correspond to those estimated in Table I. In turn, the $p + p$ reference has a factor ~10 higher statistics.

The first observation concerning Fig. 10 is that this toy model is able to generate a visible narrowing of the leading-k_t distribution at midrapidity for all p_t intervals, as was the case in the comparison to the groomed jet radius data in Ref. [15]. In agreement with the analytic results of Sec. III A 1, the ratio becomes close to one as one evolves toward more forward rapidities. Note that for the low-p_t bin the narrowing persists even at the most forward rapidity bin, since the value of f_q is smaller than for the other p_t bins. The key outcome of this exercise is that we can now quantify for which values of jet p_t and rapidity one can discriminate between our two predictions: the one based on the modified q/g fraction and that of the hybrid model with $L_{\rm res} = 0$ and $L_{\rm res} = 2/\pi T$. By comparing Figs. 9 and 10, we identify two jet selection cuts that achieve such goal: (i) $2.1 < |y| < 2.5$ and $225 < p_t < 300$ GeV and (ii) $3 < |y| < 4$ and $100 < p_t < 150$ GeV. The former is potentially accessible with the current technology of ATLAS and CMS experiments. The latter requires detector

[17]This effect is irrelevant at higher jet p_t, since they are not affected by the relatively small energy injection from the thermal soft particles.

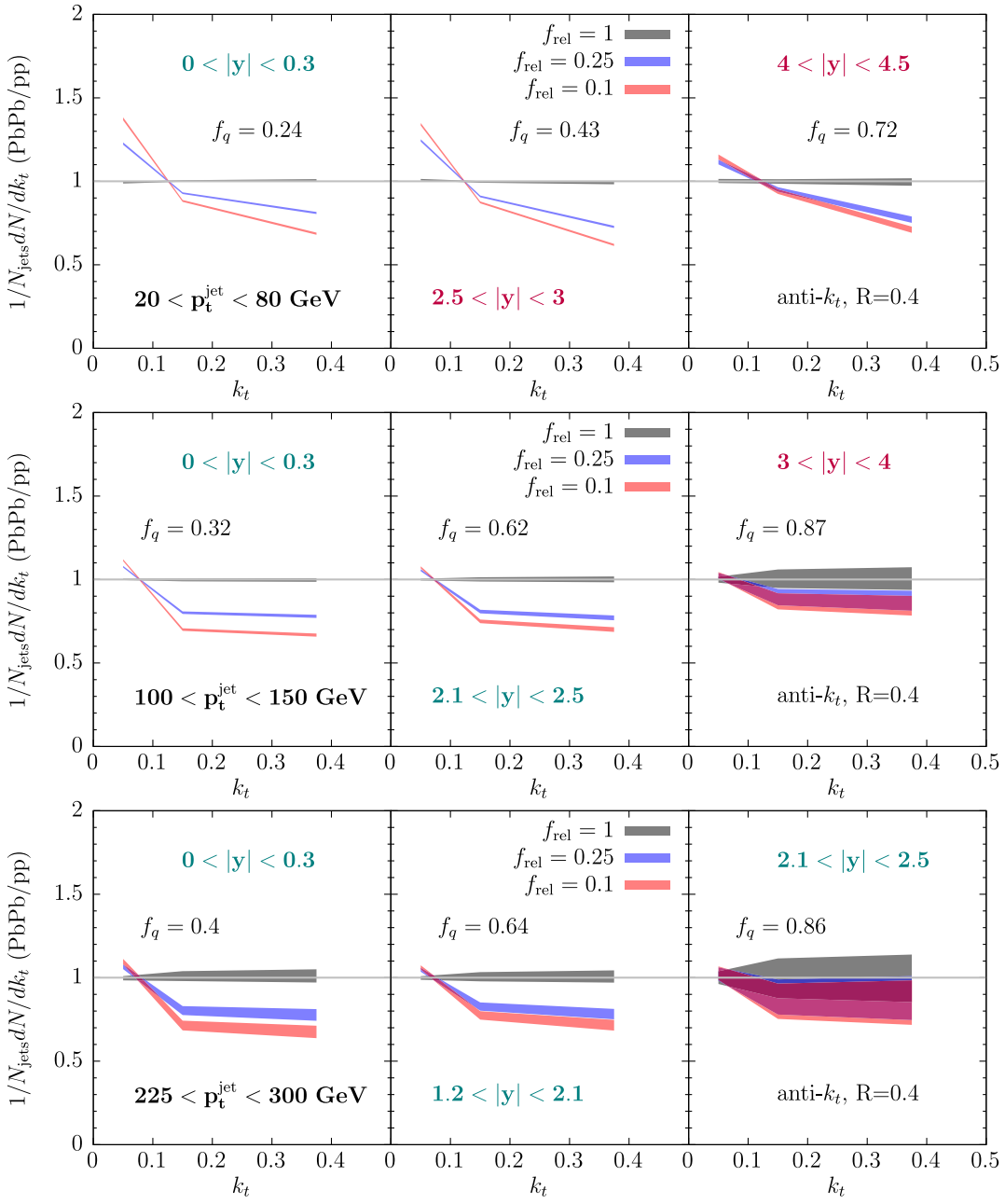

FIG. 10. Leading-k_t distribution calculated with the toy model for modified q/g fraction for different rapidity and transverse momentum intervals. The same definition of k_t as in Fig. 9 is used.

upgrades and higher statistics, so it can be targeted by all four LHC experiments beyond run 3. This is the main result of this paper.

IV. CONCLUSIONS

Jet substructure measurements at LHC energies have revealed that the hard core of the jet is narrower in heavy-ion collisions than in $p + p$. A lack of consensus exists in the theoretical interpretation of this narrowing effect. On the one hand, fully coherent energy loss models propose that a relative increase in the number of quark-initiated jets, known to possess a narrower fragmentation, with respect to vacuum suffices to explain current measurements. This increase in the number of quark-initiated jets would be based on the fact that they lose less energy than gluon-initiated jets due to their different color charge and are more likely to pass the jet p_t cut required to enter the inclusive jet ensemble. It is noteworthy that, in order to quantitatively describe the data, such a model requires a quark fraction 4 times larger than in $p + p$, a number far beyond any estimate based on the Casimir scaling of energy loss. The second category of models argue that the jet sample is

mainly dominated by unresolved splittings. That is, only sufficiently wide splittings $\theta > \theta_c$, either quark- or gluon-initiated, will be resolved by the medium, lose more energy, and make the energy of the jet they belong to fall below the p_t-selection cut.

This paper proposes a rapidity scan of jet substructure measurements to pin down the origin of the narrowing effect. We show that a gradual increase of the jet rapidity enhances the fraction of quark-initiated jets in $p + p$. Then, in a fully coherent picture of energy loss, the narrowing effect would vanish at asymptotically forward rapidities, where the flavor of the jet-initiator is fixed. In turn, the resolution scale of the medium θ_c is independent of the jet rapidity, and, thus, if the narrowing effect is driven by this phenomenon, it should persist for all rapidity values. To make these statements more quantitative, we have studied the relative transverse momentum distribution of the hardest splitting in a jet via analytic toy models and Monte Carlo simulations, the latter using the expected statistics of the high-luminosity run of the LHC. We argue that the current rapidity reach of LHC experiments at high p_t, i.e., $225 < p_t < 300$ GeV, can already access a sufficiently high q-fraction such that the different physical assumptions on the origin of the narrowing effect can be put to test. Even stronger constraints can be achieved with detector upgrades capable of measuring jet substructure at $|y| > 3$ for moderate jet p_t, i.e., $100 < p_t < 150$ GeV. This kinematic regime is well within the expected acceptance of all LHC experiments in run 4 and beyond.

Complementary constraints on the interaction of quark-initiated and gluon-initiated jets with the QGP can be obtained by the comparison of the suppression patterns of inclusive jets and (i) heavy-flavor tagged jets [95–97], which are expected to be initiated by either a charm or a bottom quark, or (ii) $Z/\gamma +$ jet events [85,94,98–104], where the quark fraction is also enhanced due to the Born level matrix element. In our opinion, measurements at forward rapidities are cleaner than these two alternative options, since the latter are subject to multiple sources of contamination. For example, a heavy-flavor tagged jet can originate from a $g \to q\bar{q}$ splitting, and so a nonvanishing fraction of g-initiated jets makes its way into the sample [105]. Equivalently, sophisticated isolation cuts are required in $\gamma +$ jet events to guarantee that the reconstructed photon was generated in the hard scattering process and not in the aftermath of the collision via electroweak radiation—and, even after applying these cuts, a sizable number of these secondary photons still persist in the final sample. Finally, Z-tagged events suffer from low statistics [106]. It would be interesting to perform a more systematic comparison of the pros and cons of these alternative methods with respect to the measurements at forward rapidities proposed in this work. We leave this task for future studies.

ACKNOWLEDGMENTS

We are grateful to Benjamin Audurier, Cristian Baldenegro, Gian Michele Innocenti, Dennis Perepelitsa, Martin Rybar, and Ricardo Vázquez for fruitful exchanges on the experimental feasibility of rapidity-dependent jet substructure measurements. We also thank Carlota Andrés for guidance on the use of the NPDF error sets. We thank Carlota Andrés, Raghav Kunnawalkam Elayavalli, Dennis Perepelitsa, Juan Rojo, Adam Takacs, and María Pía Zurita for their thoughtful comments on this manuscript. The authors thank the organizers of the XXIXth International Conference on Ultra-relativistic Nucleus-Nucleus Collisions, Quark Matter 2022, which took place in Krakow, Poland, where this collaboration started. D. P. has received funding from the European Union's Horizon 2020 research and innovation program under the Marie Skłodowska-Curie Grant Agreement No. 754496. A. S.-O.'s work was supported by the European Research Council (ERC) under the European Union's Horizon 2020 research and innovation program (Grant Agreement No. 788223, PanScales). She also thanks the Munich Institute for Astro-, Particle and BioPhysics (MIAPbP), funded by the Deutsche Forschungsgemeinschaft (DFG, German Research Foundation) under Germany's Excellence Strategy—EXC-2094—390783311, for hospitality while this publication was finalized.

[1] G. Baym, Nucl. Phys. **A956**, 1 (2016).
[2] W. Busza, K. Rajagopal, and W. van der Schee, Annu. Rev. Nucl. Part. Sci. **68**, 339 (2018).
[3] K. Adcox *et al.* (PHENIX Collaboration), Phys. Rev. Lett. **88**, 022301 (2002).
[4] C. Adler *et al.* (STAR Collaboration), Phys. Rev. Lett. **89**, 202301 (2002).
[5] J. Adam *et al.* (STAR Collaboration), Phys. Rev. C **102**, 054913 (2020).
[6] J. Adam *et al.* (ALICE Collaboration), Phys. Lett. B **746**, 1 (2015).
[7] V. Khachatryan *et al.* (CMS Collaboration), Phys. Rev. C **96**, 015202 (2017).
[8] M. Aaboud *et al.* (ATLAS Collaboration), Phys. Lett. B **790**, 108 (2019).
[9] A. M. Sirunyan *et al.* (CMS Collaboration), J. High Energy Phys. 05 (2021) 284.
[10] D. d'Enterria, Landolt-Bornstein **23**, 471 (2010).

[11] A. Majumder and M. Van Leeuwen, Prog. Part. Nucl. Phys. **66**, 41 (2011).
[12] Y. Mehtar-Tani, J. G. Milhano, and K. Tywoniuk, Int. J. Mod. Phys. A **28**, 1340013 (2013).
[13] A. M. Sirunyan *et al.* (CMS Collaboration), Phys. Rev. Lett. **120**, 142302 (2018).
[14] S. Acharya *et al.* (ALICE Collaboration), Phys. Lett. B **802**, 135227 (2020).
[15] S. Acharya *et al.* (A Large Ion Collider Experiment, ALICE Collaborations), Phys. Rev. Lett. **128**, 102001 (2022).
[16] L. Cunqueiro and A. M. Sickles, Prog. Part. Nucl. Phys. **124**, 103940 (2022).
[17] C. L. Basham, L. S. Brown, S. D. Ellis, and S. T. Love, Phys. Rev. Lett. **41**, 1585 (1978).
[18] C. Andres, F. Dominguez, R. Kunnawalkam Elayavalli, J. Holguin, C. Marquet, and I. Moult, arXiv:2209.11236.
[19] ATLAS Collaboration, arXiv:2211.11470.
[20] M. Spousta and B. Cole, Eur. Phys. J. C **76**, 50 (2016).
[21] F. Ringer, B.-W. Xiao, and F. Yuan, Phys. Lett. B **808**, 135634 (2020).
[22] ALICE Collaboration, arXiv:2204.10270.
[23] J.-W. Qiu, F. Ringer, N. Sato, and P. Zurita, Phys. Rev. Lett. **122**, 252301 (2019).
[24] J. Brewer, J. Thaler, and A. P. Turner, Phys. Rev. C **103**, L021901 (2021).
[25] A. M. Sirunyan *et al.* (CMS Collaboration), J. High Energy Phys. 07 (2020) 115.
[26] H. T. Li and I. Vitev, Phys. Rev. D **101**, 076020 (2020).
[27] L. Apolinário, J. a. Barata, and G. Milhano, Eur. Phys. J. C **80**, 586 (2020).
[28] Y. Mehtar-Tani, C. A. Salgado, and K. Tywoniuk, Phys. Rev. Lett. **106**, 122002 (2011).
[29] Y. Mehtar-Tani, C. A. Salgado, and K. Tywoniuk, Phys. Lett. B **707**, 156 (2012).
[30] J. Casalderrey-Solana and E. Iancu, J. High Energy Phys. 08 (2011) 015.
[31] Y. Mehtar-Tani and K. Tywoniuk, J. High Energy Phys. 01 (2013) 031.
[32] J. Casalderrey-Solana, Y. Mehtar-Tani, C. A. Salgado, and K. Tywoniuk, Phys. Lett. B **725**, 357 (2013).
[33] L. Apolinário, N. Armesto, J. G. Milhano, and C. A. Salgado, J. High Energy Phys. 02 (2015) 119.
[34] U. A. Wiedemann, Nucl. Phys. **B588**, 303 (2000).
[35] M. Gyulassy, P. Levai, and I. Vitev, Phys. Rev. Lett. **85**, 5535 (2000).
[36] M. D. Sievert and I. Vitev, Phys. Rev. D **98**, 094010 (2018).
[37] Y. Mehtar-Tani, C. A. Salgado, and K. Tywoniuk, J. High Energy Phys. 04 (2012) 064.
[38] J. Casalderrey-Solana, D. Pablos, and K. Tywoniuk, J. High Energy Phys. 11 (2016) 174.
[39] P. Caucal, E. Iancu, A. H. Mueller, and G. Soyez, Phys. Rev. Lett. **120**, 232001 (2018).
[40] P. Caucal, E. Iancu, and G. Soyez, J. High Energy Phys. 10 (2019) 273.
[41] J. Casalderrey-Solana, D. C. Gulhan, J. G. Milhano, D. Pablos, and K. Rajagopal, J. High Energy Phys. 10 (2014) 019; 09 (2015) 175(E).
[42] Z. Hulcher, D. Pablos, and K. Rajagopal, J. High Energy Phys. 03 (2018) 010.
[43] J. Casalderrey-Solana, G. Milhano, D. Pablos, and K. Rajagopal, J. High Energy Phys. 01 (2020) 044.
[44] K. Zapp, G. Ingelman, J. Rathsman, J. Stachel, and U. A. Wiedemann, Eur. Phys. J. C **60**, 617 (2009).
[45] K. C. Zapp, Eur. Phys. J. C **74**, 2762 (2014).
[46] M. Spousta and B. Cole, Eur. Phys. J. C **76**, 50 (2016).
[47] H. Bossi (ALICE Collaboration), Acta Phys. Pol. B Proc. Suppl. **16**, 64 (2023).
[48] J. Brandenburg, Proc. Sci. HardProbes2020 (**2021**) 179.
[49] M. Aaboud *et al.* (ATLAS Collaboration), Phys. Rev. C **98**, 024908 (2018).
[50] A. M. Sirunyan *et al.* (CMS Collaboration), J. High Energy Phys. 05 (2019) 043.
[51] V. Khachatryan *et al.* (CMS Collaboration), J. Instrum. **16**, P02010 (2021).
[52] Z. Citron *et al.*, CERN Yellow Rep. Monogr. **7**, 1159 (2019).
[53] ALICE Collaboration, Letter of intent for ALICE 3: A next generation heavy-ion experiment at the LHC, CERN Technical Report No. CERN-LHCC-2022-009 and CERN-LHCC-2017-023, 2022.
[54] CMS Collaboration, The phase-2 upgrade of the CMS endcap calorimeter, Technical Report No. CMS-TDR-019, 2017.
[55] ATLAS Collaboration, Expected tracking and related performance with the updated ATLAS Inner Tracker layout at the High-Luminosity LHC, Technical Report, 2021.
[56] C. Bierlich *et al.*, SciPost Phys. Codebases **8**, (2022).
[57] P. Caucal, A. Soto-Ontoso, and A. Takacs, Phys. Rev. D **105**, 114046 (2022).
[58] M. Cacciari, G. P. Salam, and G. Soyez, J. High Energy Phys. 04 (2008) 063.
[59] M. Cacciari, G. P. Salam, and G. Soyez, Eur. Phys. J. C **72**, 1896 (2012).
[60] Y. Mehtar-Tani, A. Soto-Ontoso, and K. Tywoniuk, Phys. Rev. D **101**, 034004 (2020).
[61] P. Caucal, A. Soto-Ontoso, and A. Takacs, J. High Energy Phys. 07 (2021) 020.
[62] ALICE Collaboration, arXiv:2204.10246.
[63] Y. L. Dokshitzer, G. D. Leder, S. Moretti, and B. R. Webber, J. High Energy Phys. 08 (1997) 001.
[64] K. J. Eskola, P. Paakkinen, H. Paukkunen, and C. A. Salgado, Eur. Phys. J. C **77**, 163 (2017).
[65] J. Casalderrey-Solana, D. C. Gulhan, J. G. Milhano, D. Pablos, and K. Rajagopal, J. High Energy Phys. 03 (2016) 053.
[66] L.-G. Pang, H. Petersen, and X.-N. Wang, Phys. Rev. C **97**, 064918 (2018).
[67] R. Baier, Y. L. Dokshitzer, A. H. Mueller, and D. Schiff, J. High Energy Phys. 09 (2001) 033.
[68] F. D'Eramo, K. Rajagopal, and Y. Yin, J. High Energy Phys. 01 (2019) 172.
[69] R. Ehlers (ALICE Collaboration), Proc. Sci. Hard-Probes2020 (**2021**) 146.
[70] Z. Hulcher, D. Pablos, and K. Rajagopal, Acta Phys. Pol. B Proc. Suppl. **16**, 57 (2023).

[71] Y. Mehtar-Tani and K. Tywoniuk, Phys. Rev. D **98**, 051501 (2018).
[72] J. Barata, P. Caucal, J. Isaaksen, A. Soto-Ontoso, A. Takacs, and K. Tywoniuk (to be published).
[73] K. Zapp, Phys. Lett. B **835**, 137567 (2022).
[74] P. M. Chesler and K. Rajagopal, Phys. Rev. D **90**, 025033 (2014).
[75] P. M. Chesler and K. Rajagopal, J. High Energy Phys. 05 (2016) 098.
[76] J. Casalderrey-Solana, Z. Hulcher, G. Milhano, D. Pablos, and K. Rajagopal, Phys. Rev. C **99**, 051901 (2019).
[77] J. Casalderrey-Solana, D. Gulhan, G. Milhano, D. Pablos, and K. Rajagopal, J. High Energy Phys. 03 (2017) 135.
[78] J. Casalderrey-Solana, J. G. Milhano, D. Pablos, K. Rajagopal, and X. Yao, J. High Energy Phys. 05 (2021) 230.
[79] Y. Tachibana, N.-B. Chang, and G.-Y. Qin, Phys. Rev. C **95**, 044909 (2017).
[80] D. Pablos, Phys. Rev. Lett. **124**, 052301 (2020).
[81] D. Pablos, Proc. Sci. HardProbes2020 (**2021**) 147.
[82] Y. Mehtar-Tani, D. Pablos, and K. Tywoniuk, Phys. Rev. Lett. **127**, 252301 (2021).
[83] J. Casalderrey-Solana, G. Milhano, D. Pablos, and K. Rajagopal, Nucl. Phys. **A1005**, 121904 (2021).
[84] K. Rajagopal, A. V. Sadofyev, and W. van der Schee, Phys. Rev. Lett. **116**, 211603 (2016).
[85] J. Brewer, Q. Brodsky, and K. Rajagopal, J. High Energy Phys. 02 (2022) 175.
[86] Y.-L. Du, D. Pablos, and K. Tywoniuk, J. High Energy Phys. 03 (2020) 206.
[87] G. Milhano, U. A. Wiedemann, and K. C. Zapp, Phys. Lett. B **779**, 409 (2018).
[88] S. S. Gubser, D. R. Gulotta, S. S. Pufu, and F. D. Rocha, J. High Energy Phys. 10 (2008) 052.
[89] Y. He, S. Cao, W. Chen, T. Luo, L.-G. Pang, and X.-N. Wang, Phys. Rev. C **99**, 054911 (2019).
[90] S. P. Adhya, C. A. Salgado, M. Spousta, and K. Tywoniuk, Eur. Phys. J. C **82**, 20 (2022).
[91] P. Caucal, E. Iancu, and G. Soyez, J. High Energy Phys. 04 (2021) 209.
[92] K. J. Eskola, P. Paakkinen, H. Paukkunen, and C. A. Salgado, Eur. Phys. J. C **82**, 413 (2022).
[93] R. Abdul Khalek, R. Gauld, T. Giani, E. R. Nocera, T. R. Rabemananjara, and J. Rojo, Eur. Phys. J. C **82**, 507 (2022).
[94] A. Takacs and K. Tywoniuk, J. High Energy Phys. 10 (2021) 038.
[95] S. Chatrchyan *et al.* (CMS Collaboration), Phys. Rev. Lett. **113**, 132301 (2014); **115**, 029903(E) (2015).
[96] ALICE Collaboration, arXiv:2208.04857.
[97] H. T. Li and I. Vitev, Phys. Lett. B **793**, 259 (2019).
[98] J. Gallicchio and M. D. Schwartz, J. High Energy Phys. 10 (2011) 103.
[99] X.-N. Wang and Y. Zhu, Phys. Rev. Lett. **111**, 062301 (2013).
[100] M. Aaboud *et al.* (ATLAS Collaboration), Phys. Rev. Lett. **123**, 042001 (2019).
[101] A. M. Sirunyan *et al.* (CMS Collaboration), Phys. Rev. Lett. **121**, 242301 (2018).
[102] Z.-B. Kang, I. Vitev, and H. Xing, Phys. Rev. C **96**, 014912 (2017).
[103] G. Aad *et al.* (ATLAS Collaboration), Phys. Rev. Lett. **126**, 072301 (2021).
[104] Z. Yang, W. Chen, Y. He, W. Ke, L. Pang, and X.-N. Wang, Phys. Rev. Lett. **127**, 082301 (2021).
[105] M. Attems, J. Brewer, G. M. Innocenti, A. Mazeliauskas, S. Park, W. van der Schee, and U. Wiedemann, arXiv:2209.13600.
[106] A. M. Sirunyan *et al.* (CMS Collaboration), Phys. Rev. Lett. **128**, 122301 (2022).